20 mW, 70 nm bandwidth ASE fibre optic source at 1060 nm wavelength region for Optical Coherence Tomography

Irina Trifanov[*], Paulo Caldas[(a)], Liviu Neagu, Rosa Romero, Martin O. Berendt, José R. Salcedo, Adrian Gh. Podoleanu[(b)], António B. Lobo Ribeiro[(c)]

Multiwave Photonics S.A., R. Eng. Frederico Ulrich 2650, 4470-605 Moreira da Maia, Portugal
(a) UOSE, INESC-Porto, Dept. Physics, Faculdade de Ciências da Universidade do Porto, R. Campo Alegre 687, 4150-179 Porto, Portugal.
(b) Applied Optics Group, School of Physical Sciences, University of Kent, Canterbury, Kent CT2 7NR, U.K.
(c) Also with: Faculty of Health Sciences, University Fernando Pessoa, R. Carlos da Maia 296, 4200-150 Porto, Portugal.

ABSTRACT

Optical coherence tomography (OCT) imaging at 1060 nm region proved to be a successful alternative in ophthalmology not only for resolving intraretinal layers, but also for enabling sufficient penetration to monitor the sub-retinal vasculature in the choroids when compared to most commonly used OCT imaging systems at 800 nm region. To encourage further clinical research at this particular wavelength, we have developed a compact fiber optic source based on amplified spontaneous emission (ASE) centered at ~1060 nm with ~70 nm spectral bandwidth at full-width half maximum (FWHM) and output power >20 mW. Our approach is based on a combination of slightly shifted ASE emission spectra from a combination of two rare-earth doped fibers (Ytterbium and Neodymium). Spectral shaping and power optimization have been achieved using in-fiber filtering solutions. We have tested the performances of the source in an OCT system optimized for this wavelength.

Keywords: broadband sources, amplified spontaneous emission, optical coherence tomography.

1. INTRODUCTION

Broadband sources (BBSs) are commonly used in a wide range of applications in optical communication systems and biophotonics. They are key elements for biomedical imaging techniques such as optical coherence tomography (OCT), because an OCT system's axial resolution is given ultimately by the coherence properties of the light source. In a fully dispersion compensated OCT system, the maximum achievable axial resolution is given by the relation:

$$\Delta z = 0.44 \frac{\lambda_0^2}{\Delta\lambda} \tag{1}$$

where Δz is the depth resolution, λ_0^2 represents the central wavelength and $\Delta\lambda$ is the bandwidth at full-width half maximum (FWHM) of the source. The imaging benefits of this technology have advanced fast since 1991[1], from industrial to biomedical application, 50% of which being today in ophthalmology. Its 3D, non-invasive, non-contact, in-vivo and real-time imaging capabilities makes OCT ideally suited to imaging solutions to replace biopsy and histopathology.

[*] Email contact: itrifanov@multiwavephotonics.com

The most commonly used light sources in commercial OCT systems for ophthalmology have been superluminescent diodes (SLDs) centred either at 800 nm or 1300 nm wavelength. However, recent developments on broadband optical sources emitting at 1050 nm wavelength region have revealed enhanced depth penetration into the choroid[2,3,4] reduced scattering losses and improved image performances in eyes with turbid media[5] as well as visualization of the blood flow in the choroid[6], when compared to the most commercial used semiconductor optical source technology at 820 nm.

To improve the resolution at this wavelength a broader spectrum is needed (based on eq.(1)); this can be obtained by combining sources with different centre wavelengths to obtain a cumulative broad emission spectrum. Compound broadband amplified spontaneous emission (ASE) fibre sources based on different combinations of rare-earth doped fibres[7,8,9], or semiconductor optical amplifiers and doped fibre[10], and SLD-based combined light sources[11,12] have been developed mostly at 0.8 µm, 1.3 µm, 1.5 µm and lately 1 µm. One prior approach to obtain ASE broadband spectrum at 1 µm wavelength region with high level of power and spectral stability combines Yb-doped fibres having different glass host and dopants concentration, pumped with laser diodes at the same emission wavelength[13]. This source expands the traditional Yb-doped silica ASE (centred at 1060 nm) to shorter wavelengths side (centred at 1020 nm). However, experimental and theoretical studies have shown that better overlap of the centre wavelength and bandwidth with the water absorption window[14], meaning: central wavelength around 1060-1070 nm and bandwidth > 70 nm would further increase the penetration depth[15] and allow for maximum achievable ultra high resolution OCT imaging at this wavelength in case of the human eye[16].

2. METHOD

Figure 1a illustrates the output spectrum of an Yb-doped fiber ASE source (model BBS-1um-25-U from Multiwave Photonics SA, Portugal) centred at ~1047 nm, with FWHM of 50 nm bandwidth and 25 mW of output power.[17]

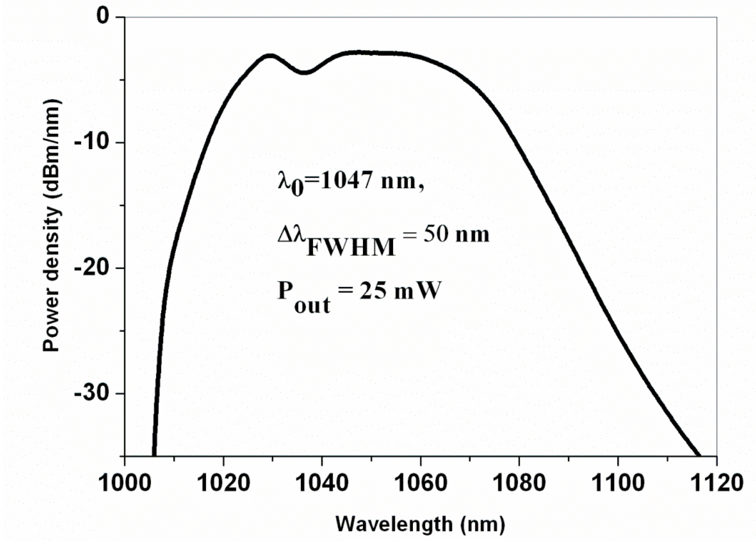

Figure 1. Output spectra of the Yb–doped fiber ASE source.

Based on our previous results[18], the addition of the emissions of two slightly displaced ASE spectra originating from different rare earth-doped fibres pumped accordingly provides a simple and robust approach for spectrum broadening. A good candidate for broadening the spectrum of Ytterbium, especially towards longer wavelengths range, is Nd-doped fiber. Nd-doped silica-based fibers have been used to demonstrate both single and double-pass ASE operating on the $^4F_{3/2} \rightarrow {}^4I_{11/2}$ transition at 1060 nm with a relative broad emission.[19] In this study, we have used a single mode Nd-doped alumino-germano-phospho-silicate fiber having 500 ppm Nd^{3+} ion concentration, 5 µm core diameter, 0.14 numerical aperture (NA).

The experimental set-up of a double-pass backward ASE configuration is shown in Figure 2a. A pump source, e.g. at 808 nm single-mode pump diode with ~100 mW maximum power is coupled into ~5m Nd-doped of fibre through the wavelength division multiplexer fibre coupler (WDM). A gold mirror (M) is placed at the end of the doped fibre permitting the collection of both amplified forward and backward ASE. The isolator (ISO) at the end prevents any reflections from returning into the ASE fibre. As plotted in Figure 2b, the emission spectrum of the Nd ASE source is asymmetric, with central peak at 1060 nm which limits its bandwidth at -3dB to about 9 nm. The source emits 20 mW with 90 mW of absorbed pump power.

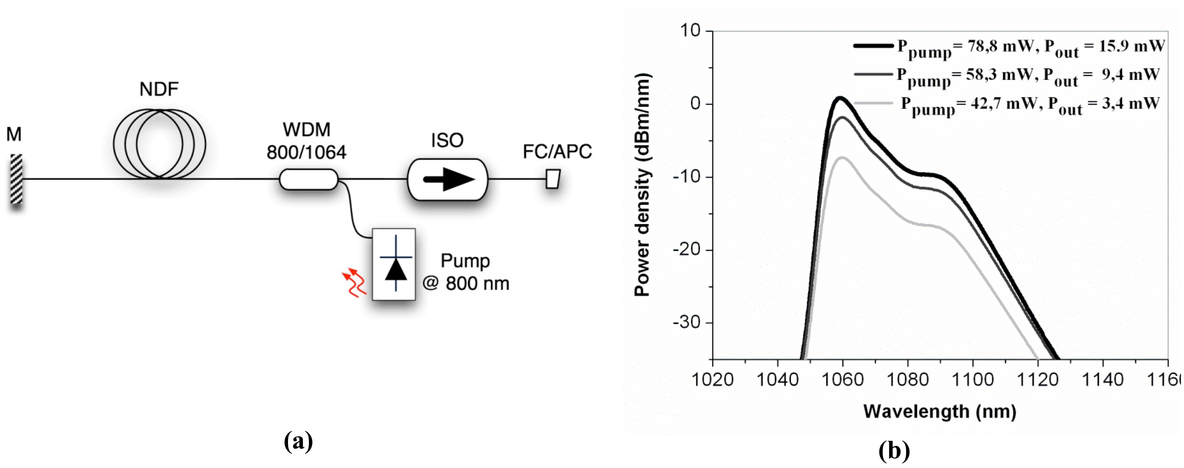

Figure 2. (a) Experimental setup of a double-pass backward Nd-doped fibre ASE source. Gold mirror (M), 800 nm pump laser diode (Pump), wavelength division multiplexer fiber coupler (WDM), Nd-doped fiber (NDF), optical isolator (ISO), fiber connector angle polished contact (FC/APC). **(b)** Output spectra of the source, for different pump levels.

The addition of the two emissions in a broadband coupler, as shown in Figure 3, can be effective due to the spectrum shift between the Nd-doped and Yb-doped silica fibres ASE emissions. The splitting ratio of the coupler (30/70) is chosen in order to balance and to achieve the maximum optical powers contributions possible from both doped fibres.

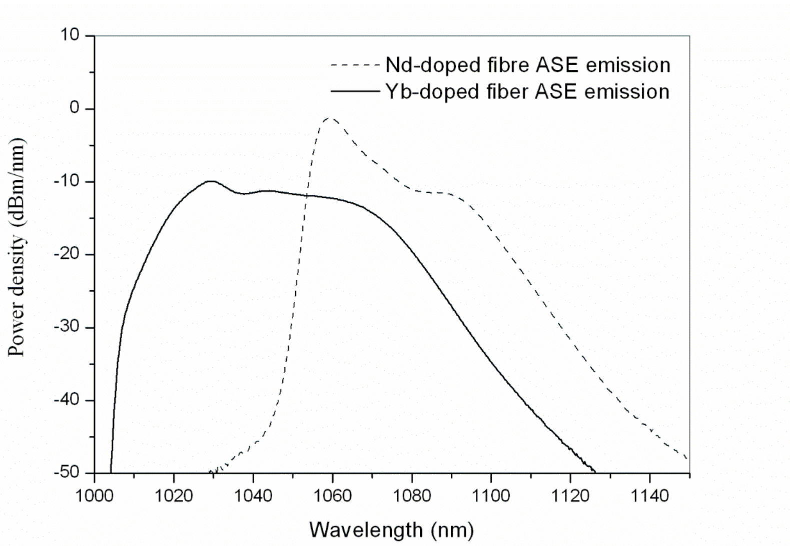

Figure 3. Measured spectrum for combined Nd-doped fiber ASE and Yb-doped fibre ASE sources.

However, a desired output spectrum (i.e Gaussian) is only achievable by means of some kind of spectral shaping. These wavelength-dependent loss elements would be ideally achieved in all-fibre technology, working in transmission and conferring maximum mechanical stability to the complete device. In the following, a study of the filtering of the Nd ASE source will be provided with the purpose of establishing the optimum parameters required in obtaining the broadest spectral range when combined with Yb-doped ASE emission spectrum previously discussed.

2.1 Spectral tailoring of Nd-doped ASE source using long period gratings

Most of the shaping studies using long period gratings (LPGs) refer to broadening and/or smoothing the Er-doped broadband sources centred at 1.55µm, because of their high impact in telecommunication industry. The position of this fibre grating can be chosen either at the end (post filtering) or in between segments of rare-earth doped fibre.[20,21]

The simplest way to shape the output spectrum is through a filter with the inverse spectrum. We simulated the shape of an ideal filter that will give more than 70 nm in bandwidth and less than 2 dB ripples for the combined spectra and plotted in Figure 4. We consider this shape as a reference for designing the filter. The spectral filtering is mainly ought to reduce the leading peak of Nd-doped fibre ASE around 1060 nm

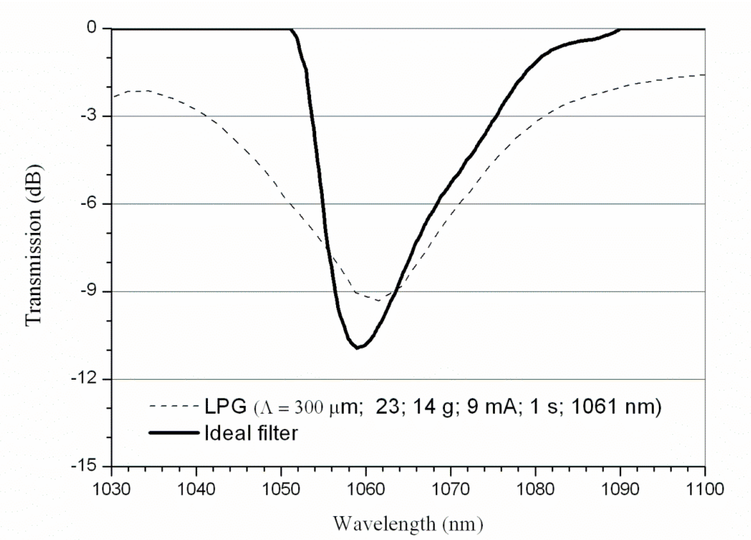

Figure 4. Transmission spectrum of the LPG (grating period, no. of discharges, mass attached, intensity of the arc discharge, duration of the arc discharge, resonance wavelength) in comparison with the ideal filter.

The LPGs used in this study were written in HI1060 fibre and fabricated using the electric-arc technique.[22] We have tested several LPGs designed to induce an excess loss at the dominant band of the original double-pass backward Nd-doped fibre ASE spectrum. The one that fitted the best spectral shape of our ideal filter is also shown in Figure 4. It has a periodicity of 300 µm and an overall length of 6.9 cm. The peak coupling to a cladding mode occurred at a wavelength of 1061 nm, approximately matching the peak and exceeding the bandwidth of the ideal filter.

The LPG was then placed in different positions of the combined Nd-Yb doped ASE source:

(1) At the end of a double pass configuration (post-filtering); the output spectrum and the output power will both follow the characteristics of the filter, which means that shaping is achieved with a significant decrease of output power.

(2) In a double pass configuration and is meant to filter only the ASE in one direction, which upon reflection will seed the ASE emitted in the other direction; this has a significant effect on reducing the power losses and most importantly in redistributing the power from the dominant band to other spectral ranges[23]. This effect results from gain saturation induced by the seeded signal, and has also as a consequence an increase in the lasing threshold.

In terms of optical power losses, Figure 5a illustrates the dependence of the output power with the pump power for both positions of the LPG in comparison with the original, unfiltered ASE. It can be easily noticed that the power efficiency in position (2) follows the curve of the unfiltered configuration within a loss of less than 30 % at maximum pump power (mainly due to the LPG insertion loss), while in position (1) the power decreases drastically, as expected. Figure 5b shows the effect of the filtered ASE seeding on the forward output spectrum as compared to post-filtering. Significant spectral reshaping and broadening especially towards longer wavelength range is achieved for the same pump power (P_{pump} =78.8 mW).

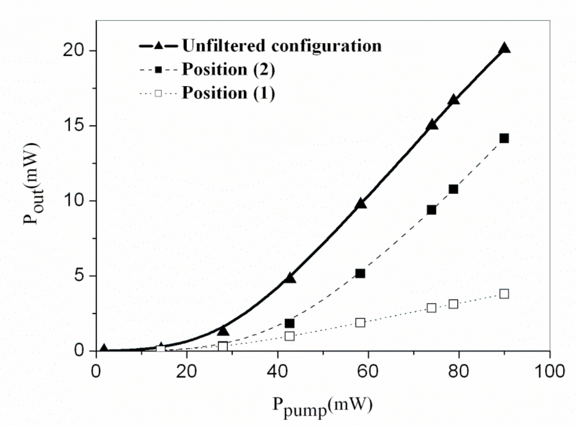

(a)

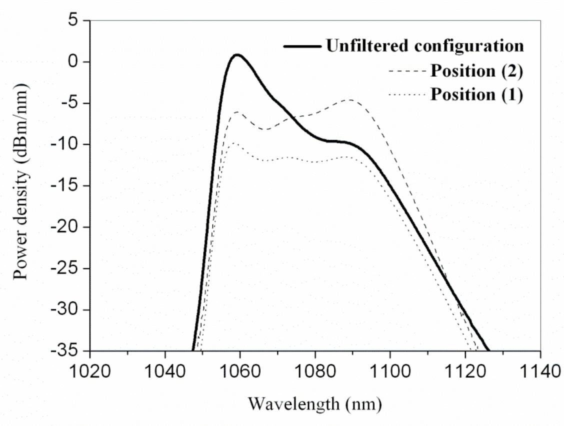

(b)

Figure 5. (a) Output power as a function of pump power for each position of the filter in comparison with the unfiltered configuration; **(b)** Output spectra of unfiltered double pass backward Nd-doped ASE in comparison with the filtered configurations.

We have also performed studies in terms of central wavelength and bandwidth stability with pump power for this particular filter in both cases. Figure 6a shows that the central wavelength tends to stabilize within less than 1 nm within the high-pump power region for the situation with the filter in position (2). Moreover, the redistribution of power towards longer wavelength range is quantitatively indicated by the values of the central wavelength in comparison with filter in position (1). In terms of bandwidth as seen in Figure 6b, although a slightly broader bandwidth can be obtained in the high-pump power region with the filter in position (1), it tends to decrease and the output power is too small for our application. Again, the configuration with the filter in position (2) shows very good stability in terms of bandwidth for high-pump power region.

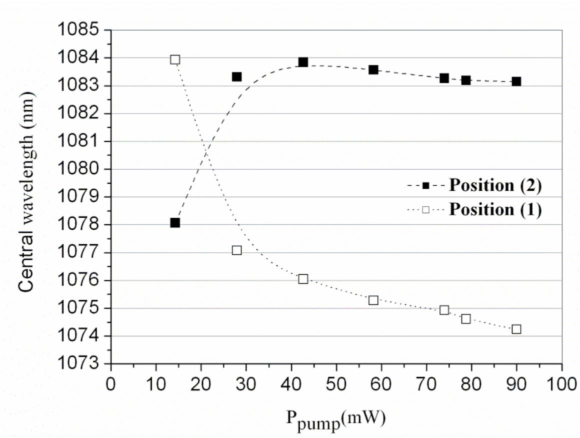

(a)

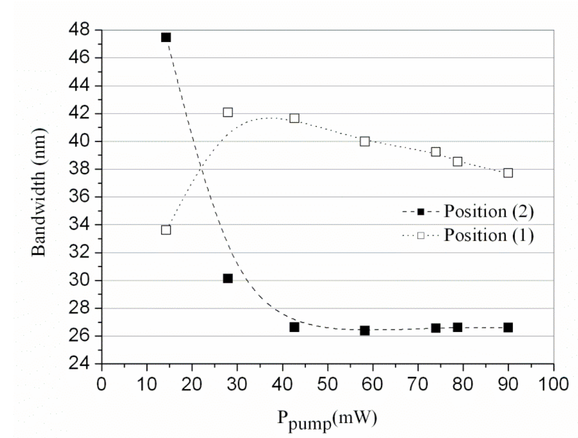

(b)

Figure 6. Measured central wavelength **(a)** and bandwidth **(b)** versus pump power for the different positions of the filter.

Overall, the configuration with the filter in position (2) matches better our requirements in terms of bandwidth, central wavelength and output power when combined with Yb-doped ASE source. However, a number of improvements can be performed in terms of insertion loss of the filter and the position and excess loss of the resonance.

2.2 Extended broadband ASE source at 1 micron characterization for OCT imaging

Figure 7a shows the output spectrum of the extended Broadband ASE Source (eBBS) based on ASE from a diode-pumped Nd-doped and Yb-doped fibre combination as previously discussed.[24] This source delivers more than 20 mW non polarized power in single transverse mode, centred on 1060 nm wavelength with a spectral bandwidth (FWHM) of more than 70 nm.

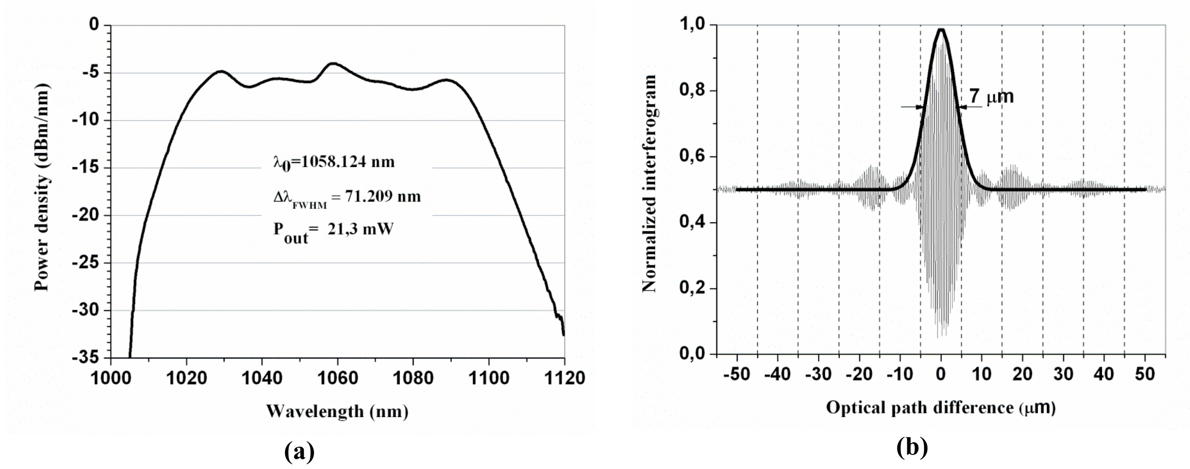

Figure 7. (a) Output spectrum of extended broadband ASE source; (b) Normalized interferogram

In addition to the primary source criteria of wavelength, bandwidth, and power, a specific spectral shape or the distribution of the source power spectrum has significant importance for OCT applications. Mathematically, the inverse Fourier transform of the source power spectrum gives the autocorrelation function (Wiener-Khitchin theorem). We have measured it using a Michelson interferometer wavelength meter (HP 8612B) modified to give access for measurement to two detector signals to be connected to an oscilloscope. One detector signal gives the reference from a known, stabilized laser source to calibrate the interferometer's mirror movement accurately. The other detector measures the optical interferogram of the source under test. The autocorrelation function of the source is shown in Figure 7b. This measurement provides two significant aspects in terms of imaging applications:

(1) It proves that in a fully dispersion compensated OCT system optimized for this wavelength range, the source would give an axial resolution of 7 μm in air ~ 5 μm in tissue (n_{tissue}=1.4), confirmed also by the theory (eq. (1));

(2) It shows that the autocorrelation function has secondary peaks or side lobes (less than 10 % of the main peak in magnitude) due to the non-Gaussian profile.

Although it is generally accepted that the ideal spectral shape for an OCT system is Gaussian, the spectral shape of most reported broadband sources has been far from Gaussian. The deviation of the spectrum of our source from Gaussian can cause severe coherent artefacts in the image because of the presence of side-lobes in the fringe pattern symmetrically to the autocorrelation function maximum. Post-processing of the coherence function (after registration of the full interferogram) has been employed to minimize this unwanted effect, but is problematic for real-time operation. Moreover, a study on the maximum permissible value of side lobes could have a great significance for image interpretation.

Other issues like: portability, ease of use, compatibility with the application environment make this source suitable for simple integration in an OCT system optimized at this wavelength range for in situ or in vivo imaging applications.

3. APPLICATION. OCT IMAGING

The source has been properly packaged and tested in a time-domain OCT system optimized for this wavelength range[25]. The system is capable of acquiring *en-face* as well as cross sectional OCT images. A confocal channel was also implemented by diverting a small part of the signal returning from the sample into a Silicon avalanche photodetector. The main advantage of the OCT over the confocal microscopy is that OCT achieves very high axial image resolution, independent of the focusing condition, while the lateral resolution is practically the same in both imaging modalities and is defined by the focal spot size.[26]

In all subsequent retinal OCT images, the axial resolution is given by the coherence length of the source multiplied by the transfer function of the OCT system. The measured value is about 15 μm in tissue; therefore the resolution is smaller than the theoretical one, probably due to unbalance dispersion or polarization effects in the OCT system. The lateral resolution is limited by the beam diameter and the optics of the eye to about ~15 μm. The power incident on the cornea was 3 mW, which is below the maximum permissible exposure limits recommended by the ANSI standard.[27]

A cross sectional *in vivo* OCT image of the eye fundus at 1060 nm is shown in Figure 8a, showing well defined retinal layers as well as superior penetration into the choroid due to improved penetration at longer wavelength. The image size is 3 x 3 mm.

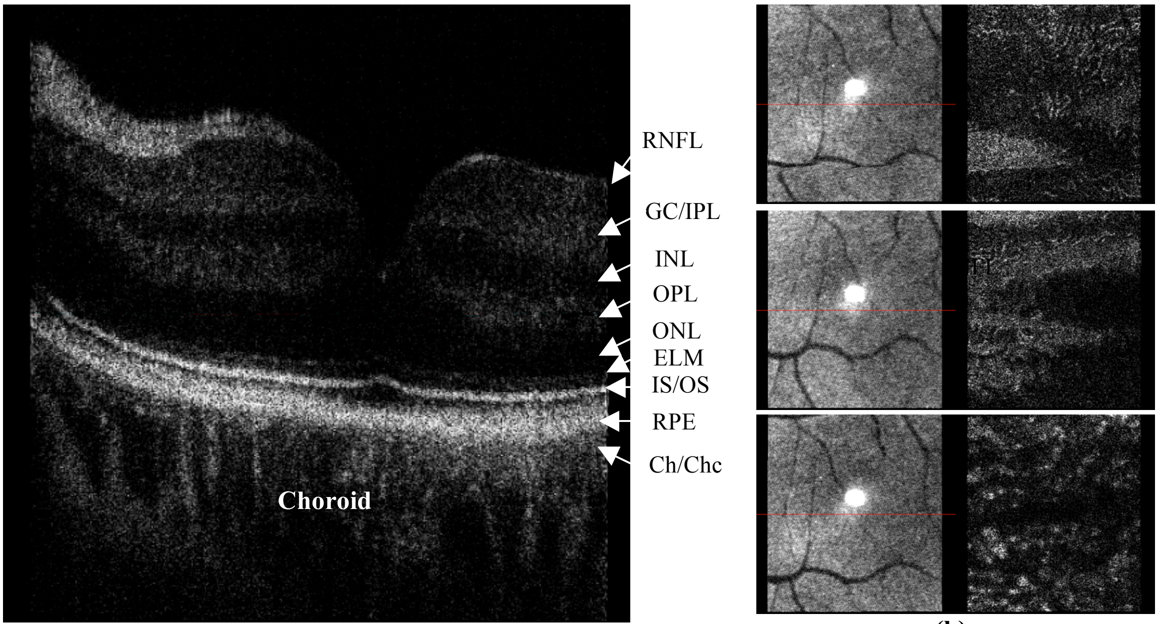

(a) **(b)**

Figure 8. (a) Cross sectional *in vivo* OCT image of the eye fundus showing: RNFL, retinal nerve fiber layer; GC/IPL, ganglion cell/inner plexiform layer; INL, inner nuclear layer; OPL, outer plexiform layer; ONL, outer nuclear layer; ELM, external limiting membrane; IS/OS, photoreceptor inner segment/outer segment junction; RPE, retinal pigment epithelium; Ch/Chc, choroid/choriocapillaris. (b) Confocal/*en-face* OCT images of the macular region *in vivo* at different axial positions in the retina and choroid.

Pairs of confocal/*en-face* OCT images of the macular region *in vivo* acquired at different axial positions in the retina and choroid are shown in Figure 8b. The image size is 1 x 1 mm. Retinal and choroidal vasculatures are visible in the confocal images (left) superposed due to a 1 mm depth of focus. Depth resolved images are provided by the OCT channel (right). Due to a much higher depth resolution, they look fragmented. They have been acquired at different depth showing structures that we have identified as probably being from the choroid[28], although the depth was not accurately controlled. The bright, intense spot in the confocal image represents the reflection from the focusing lens.

4. CONCLUSIONS

We have developed and characterized a new, broadband ASE source at 1 micron, based on a combination of Yb-Nd doaped fibers, for OCT imaging of human retina. Higher power, broader ASE bandwidth and smoother spectrum are subjected to increasing the pump power and/or designing a filter that will match the characteristics of the ideal one.

ACKNOWLEDGEMENTS

This project is granted from Marie Curie training site supported by the European Commission under the project HIRESOMI (project: Marie Curie EC MEST-CT-2005-020353) and in collaboration with Multiwave Photonics SA, Portugal.

REFERENCES

[1] Huang, D., Swanson, E. A, Lin W. G. S. C. P., Schuman, J. S., Chang, W., Hee, T. F. M. R., Gregory, K., Puliafito, C. A., and Fujimoto, J. G., “Optical coherence tomography,” Science 254, 1178–1181 (1991).
[2] Považay, B., Hofer, B., Torti, C., Hermann, B., Tumlinson, A. R., Esmaeelpour, M.,. Egan C. A, Bird, A. C., and Drexler, W., "Impact of enhanced resolution, speed and penetration on three-dimensional retinal optical coherence tomography," Opt. Express 17, 4134-4150 (2009).
[3] Makita, S., Fabritius, T., and Yasuno, Y., “Full-range, high-speed, high-resolution 1-μm spectral-domain optical coherence tomography using bm-scan for volumetric imaging of the human posterior eye,” Opt. Express ***16***(12), 8406–8420 (2008).
[4] Cucu, R G., Rogers, J. A.,. Hathaway, M. W, Pedro, J., Podoleanu, A. Gh., Rosen, R. B.,“Combined confocal/en face optical coherence tomography imaging of the human eye fundus in vivo in the 1050 nm spectral region” Proc. SPIE 6429, 642903-01 to 642903-05, (2007).
[5] Považay, B., Hermann, B., Unterhuber, A., Hofer, B., Sattmann, H., Zeiler, F., Morgan, J. E., Falkner-Radler, C., Glittenberg, C., Binder, S., and Drexler, W., “Three-dimensional optical coherence tomography at 1050 nm versus 800 nm in retinal pathologies: enhanced performance and choroidal penetration in cataract patients”, Journal of Biomedical Optics 12(4), 041211-(1-7) (2007).
[6] Makita, S., Fabritius, T., and Yasuno Y., “Blood flow imaging at deep posterior human eye using 1 μm spectral-domain optical coherence tomography”, Proc. SPIE 7168, 716808 (2009).
[7] Chen, H. and Schinn, G. W., “Hybrid broadband superfluorescent fiber source consisting of both thulium-doped fiber and erbium-doped fiber”, Optics Communications 229**,** 141–146 (2004).
[8] Paschotta, R., Nilsson, J., Tropper, A., and Hanna, D., “Efficient superfluorescent light sources with broad Bandwidth”, IEEE Journal of Selected Topics in Quantum Electronics, 3(4), 1097-1099 (1997).
[9] Haroud, K., Rochat, E., and Dändlicker, R., “A broad-band Superfluorescent fiber laser using single-mode doped silica fiber combinations”, IEEE Journal of Quantum Electronics, 36(2), 151-154 (2000).
[10] Beitel, D., Carrion, L., Chen, L. R., and Maciejko, R., “Development of Broadband Sources Based on Semiconductor Optical Amplifiers and Erbium-Doped Fiber Amplifiers for Optical Coherence Tomography”, IEEE Journal of Selected Topics in Quantum Electronics, 14(1), 243-250 (2008).
[11] Andreeva, E. V., Lapin, P .I., Prokhorov, V.V., Shidlovski V. R., Shramenko, M. V., and Yakubovich, S.D., “Novel Superluminescent Diodes and SLD-based Light Sources for Optical Coherence Tomography”, in Proc. SPIE 662, 7662703 (2007).
[12] Greenwood, P., Childs, D., Groom, K.M., Stevens, B.J., Hopkinson, M., Hogg, R.A., “Tuning Superluminescent Diode Characteristics for Optical Coherence Tomography Systems by Utilizing a Multicontact Device Incorporating Wavelength-Modulated Quantum Dots”, IEEE Journal of Selected Topics in Quantum Electronics (2009).
[13] Chavez-Pirson, A., Jiang, S., Tian, W., “1-μM phosphate-glass fiber amplifies spontaneous emission source”, US Patent, 7.423.803 B1 (2008).
[14] Kou, L., Labrie, D., and Chylek, P. “Refractive indices of water and ice in the 0.65- to 2.5-μm spectral range”, Applied Optics, 32(19), 3531 (1993).
[15] Unterhuber, A., Považay, B., Hermann, B. , Sattmann, H. , Chavez-Pirson, A. , Drexler, W. ,” In vivo retinal optical coherence tomography at 1040 nm - enhanced penetration into the choroid” Opt. Express, 13, 3252-3258 (2005).
[16] Hariri, S., Moayed, A. A., Hyun, C., Shidlovski, V., Dracopoulos, A., Boyd, S. and Bizheva, K., “The broadest spectral bandwidth suitable for in-vivo UHROCT imaging of human and animal retina at 1060nm”, Proc. SPIE 7168 716807-1 (2009).
[17] Sousa, J. M., Melo, M., Ferreira, L. A., Salcedo, J. R., and Berendt, M. O., “Product design issues relating to rare-earth doped fiber ring lasers and superfluorescence sources”, Proc. SPIE 6102, 610223.1-610223.12 (2006).
[18] Trifanov, I., Berendt, M. O., Salcedo, J. R., Podoleanu, A. Gh., Lobo Ribeiro, A. B., “Development of fibre optic broadband sources at 1 μm region for optical coherence tomography”, Proc. SPIE 7139, 713906 (2008).
[19] Digonnet, M. J. F., Liu, K., “Analysis of a 1060-nm Nd:SiO2 superfluorescent fiber laser”, Journal of Lightwave Technology 7, 1009-1015 (1989).
[20] Yue, H., Ou, Z., Dai, Z., Liu, Y., “Study of Spectrum Flattening of ASE Fiber Source Based on Long Period Fiber Grating”, Proc. SPIE, 6830, 68301G-1 (2007).
[21] Hodgson, C.W., Vengsarkar, A.M., “Spectrally shaped high-power amplified spontaneous emission sources incorporating long-period gratings”, Optical fiber communications, 29-30 (1996).
[22] Rego, G., Marques, P.V.S., Santos, J.L., and Salgado, H.M., “Arc-induced long-period gratings”, Fiber and Integrated Optics, 24(3-4), 245-259 (2005).

[23] Su, C. D. and Wang, L. A., “Effect of Adding a Long Period Grating in a Double-Pass Backward Er-Doped Superfluorescent Fiber Source”, Journal of Lightwave Technology, 17(10) (1999).
[24] Lobo Ribeiro, A. B., Trifanov, I., Melo, M.A.R., Berendt, M.O., Romero, R. and Salcedo J.A.R., "Broadband Neodymium-Ytterbium-Silica Doped Amplified Spontaneous Emission Optical Fiber Source by Spectral Filtered Re-injected Signals", US Patent Pending Application No.12/482670 (2009).
[25] Neagu, L., Lobo, A., Salcedo, J., Cucu, R. G., Bradu, A, Ma, L., Bloor, J., Podoleanu, A. Gh., “Frequency Shifter Based en-Face OCT System at 1060 nm”, in Proc. of the Topical Meeting on Optoinformatics of the 5th International Optical Congress, Optoinformatics’08, St. Petersburg, Rússia, 143 (2008).
[26] Podoleanu, A. Gh., Jackson, D.A., “Combined optical coherence tomograph and scanning laser ophthalmoscope”, Electron. Lett., 34(11), 1088 (1998).
[27] American National Standards Institute, ”American National Standard for Safe Use of Lasers,” ANSI Z 136-1, 2000.
[28] Povazay, B., Hermann, B., Hofer, B., Kajic, V., Simpson, E., Bridgford, T., and Drexler, W., “Wide-Field Optical Coherence Tomography of the Choroid In Vivo”, Invest. Ophthalmol. Vis. Sci. 50, 1856 – 1863 (2009).